Photocatalytic Activity for Water Decomposition of RuO_2-Dispersed Zn_2GeO_4 with d^{10} Configuration

J. Sato,[†] H. Kobayashi,[‡] K. Ikarashi,[†] N. Saito,[†] H. Nishiyama,[†] and Y. Inoue*[,†]

Department of Chemistry, Nagaoka University of Technology, Nagaoka 940-2188, Japan, and Department of Chemistry and Bioscience, Kurashiki University of Science and the Arts, Kurashiki 712-8505, Japan

Received: November 2, 2003; In Final Form: December 26, 2003

RuO_2-dispersed Zn_2GeO_4 was found to become a stable photocatalyst for the overall splitting of water to produce H_2 and O_2. The photocatalytic properties were examined under various experimental conditions, and the band structure of Zn_2GeO_4 was revealed based on the DFT calculation. The photocatalytic activity depended on calcination temperatures of Zn_2GeO_4 and the amount of RuO_2 loaded, and the combination of highly crystallized Zn_2GeO_4 with dispersed small RuO_2 particles provided large photocatalytic activity. The GeO_4 tertrahedron of Zn_2GeO_4 is so heavily distorted to generate a dipole moment inside, and the good photocatalytic performance of RuO_2-dispersed Zn_2GeO_4 is in line with the view that the electron−hole separation upon photoexcitation is promoted by a local electric field due to dipole moment. The DFT calculation showed that the top of the valence band (HOMO) was composed of the O 2p orbital, whereas the bottom of conduction band (LUMO) was formed by the Ge 4p orbital with a small contribution of the Zn 4s4p orbitals. The conduction band had large dispersion, indicative of large mobility of photoexcited electrons. The correlation of photocatalytic activity with geometric and electronic structures of Zn_2GeO_4 is discussed.

Introduction

In a series of the study[1−7] of photocatalytic properties of p-block metal oxides with d^{10} configuration, various kinds of indates (MIn_2O_4 (M = Ca,Sr), $NaInO_2$, $LaInO_3$), zinc gallate ($ZnGa_2O_4$), strontium stannate (Sr_2SnO_4), and various antimonates ($M_2Sb_2O_7$ (M = Ca, Sr), $CaSb_2O_6$, $NaSbO_3$) have been found to be photocatalytically active by loading RuO_2 for water decomposition under UV illumination. These results demonstrated that p-block metal ions with d^{10} configuration such as Ga^{3+}, In^{3+}, Sn^{4+}, and Sb^{5+} became a core element to be photocatalytically active for the reaction. In 4p and 5p block metal ions, a Ge^{4+} ion is only the remaining metal ion without investigation. The demonstration for Ge^{4+} metal oxides with d^{10} configuration leads to the establishment of a photocatalyst system consisting of 4p and 5p block metal oxides. In an attempt to reveal the photocatalytic activity of Ge metal oxides, we have first examined alkaline earth metal germanates of M_2GeO_4 (M = Ca, Sr, Ba), but unfortunately, these germanates were not stable in water under UV light illumination. Instead of alkaline earth metal oxides, Zn_2GeO_4 was found to be sable and active photocatalytically by the combination with RuO_2. The optimum conditions for good photocatalytic performance were obtained experimentally, and the nature of active sites was discussed on the basis of local geometric and electronic band structures.

By combining the present findings with previous ones, it has been established that p-block metal oxides involving Ga^{3+}, Ge^{4+}, In^{3+}, Sn^{4+}, and Sb^{5+} with d^{10} configuration form a group of an active photocatalyst for water decomposition, as opposed to a conventional photocatalyst group of transition metal ions (Ti^{4+}, Zr^{4+}, Nb^{5+}, Ta^{5+}) with d^0 configuration.[8−21]

Experimental Section

An equimolar ratio of ZnO (Nakarai tesque, GR grade) and GeO_2 (Nakarai tesque, GR grade) was mixed in an agate and calcined in air for 16 h in the temperature range 1273−1573 K. For the dispersion of RuO_2 particles on Zn_2GeO_4, Zn_2GeO_4 was impregnated with ruthenium carbonyl complex, $Ru_3(CO)_{12}$, in THF and oxidized in air at 673 K for 5 h to convert the Ru surface species to RuO_2 particles.

The details of the reaction system and procedure have been shown elsewhere.[3,4] Briefly, the photocatalytic decomposition of water was carried out in a closed gas-circulating apparatus in an Ar atmosphere under irradiation with a Hg−Xe lamp (Hamamatsu L5662-02). Photocatalyst powder of 250 mg was dispersed in distilled and ion-exchanged water and stirred by bubbling with Ar gas during the photocatalytic reaction. The amounts of H_2 and O_2 produced in the gas phase were analyzed by an on-line gas chromatograph.

The crystal structures of Zn_2GeO_4 were determined by the X-ray diffraction pattern (Rigaku RAD III). UV diffuse reflectance spectra were recorded on a UV−vis spectrometer (JASCO V-570). The scanning electron microscopic (SEM) images were obtained with Shimazu EPMA 1600. The surface area was measured by Yuasa ChemBET3000.

Band calculation was carried out using the plane wave DFT program package Castep. With the pseudo potential scheme, the valence atomic configurations, Zn, $3d^{10}4s^2$; Ge, $4s^24p^2$; O, $2s^22p$, are taken into consideration. The number of occupied bands is 156 for the unit cell construction of $(Zn_2GeO_4)_6$.

* To whom correspondence should be addressed.
[†] Nagaoka University of Technology.
[‡] Kurashiki University of Science and the Arts.

10.1021/jp0373189 CCC: $27.50
Published on Web 03/17/2004

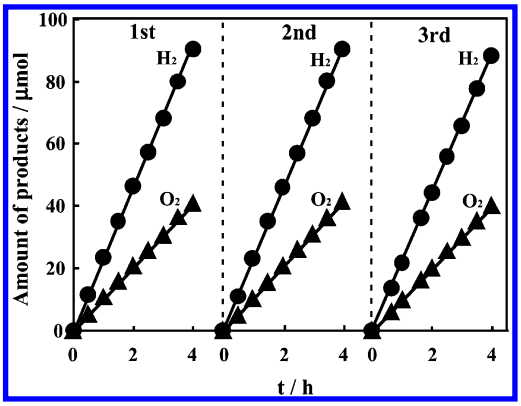

Figure 1. Production of H_2 and O_2 from water on 1.0 wt % RuO_2-dispersed Zn_2GeO_4 under UV irradiation.

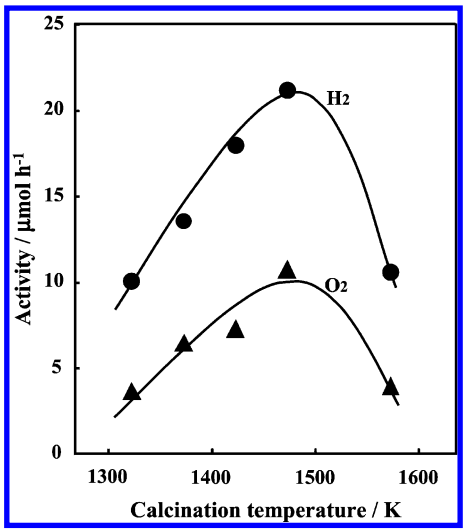

Figure 2. Photocatalytic activity of RuO_2-dispersed Zn_2GeO_4 for H_2 and O_2 production as a function of calcination temperature of Zn_2GeO_4.

Results

Figure 1 shows the reaction behavior in water decomposition on 1.0 wt % RuO_2-dispersed Zn_2GeO_4 under Hg−Xe lamp irradiation. Both hydrogen and oxygen were produced with a constant rate from the initial stage of reaction. The second and third run showed nearly the same production, and a little deterioration of photocatlaytic activity occurred. The total amount of H_2 produced in the run was larger by a factor of 260 than the number of surface Ge ions.

Figure 2 shows the dependence of photocatalytic activity on the calciantion temperature of Zn_2GeO_4. The activity increased with increasing temperature from 1323 K, reached a maximum at 1473 K, and decreased significantly. The ratio of H_2/O_2 was 2.8 for calcination temperature at 1323 K, 2.1 at 1373 K, 2.0 at 1473 K, and 2.7 at 1573 K. Figure 3 shows changes in the photocatalytic activity with the amounts of RuO_2 loaded. The large enhancement of activity occurred with increasing amount of RuO_2 below 1 wt %. The activity reached a maximum at around 1 wt %, followed by a sharp decrease with further RuO_2 loading, and reached a constant level above 2 wt %.

Figure 4 shows the X-ray diffraction patterns of Zn_2GeO_4 calcined at different temperatures. For a sample prepared at 1273 K, most of the peaks were attributed to those of Zn_2GeO_4, but small peaks due to ZnO and GeO_2 were observed. At 1373 K, these peaks relating to the unreacted oxides disappeared. Up to 1573 K, only the peaks assigned to Zn_2GeO_4 existed, indicative of a single phase of Zn_2GeO_4.

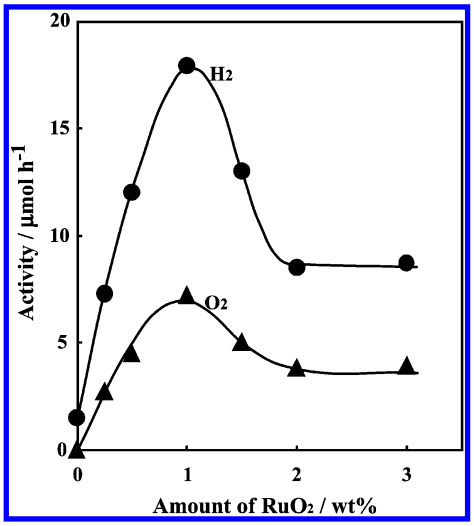

Figure 3. Changes in photocatalytic activity of RuO_2-dispersed Zn_2GeO_4 for H_2 and O_2 production with amount of RuO_2.

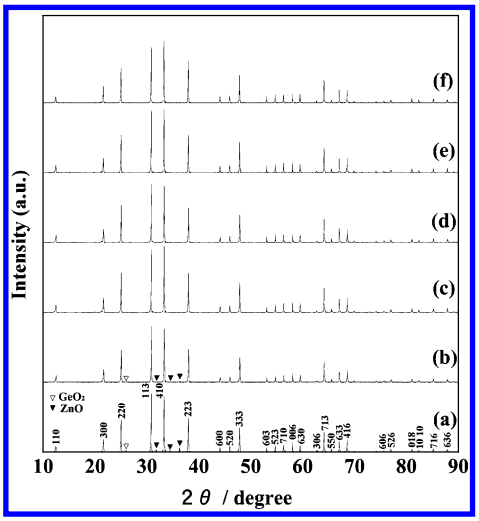

Figure 4. XRD patterns of Zn_2GeO_4 calcined at 1273 (a), 1323 (b), 1373 (c), 1423 (d), 1473 (e), and 1573 K (f).

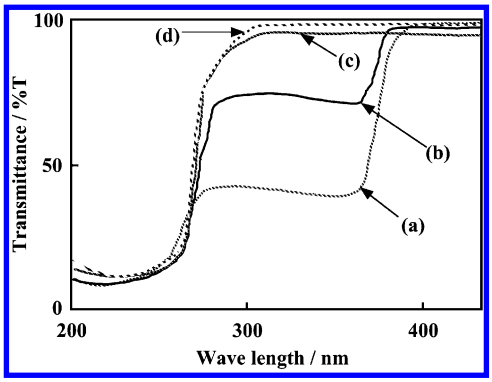

Figure 5. UV diffuse reflectance spectra of Zn_2GeO_4 calcined at 1273 (a), 1323 (b), 1473 (c), and 1573 K (d).

Figure 5 shows the UV diffuse reflectance spectra of Zn_2GeO_4 treated in the temperature range 1273−1573 K. By calcination at 1273 K, a threshold wavelength for light absorption was around 390 nm. The absorption occurred sharply and had a plateau from 370 to 270 nm. A deep absorption occurred at around 270 nm and reached the highest level at 260 nm. Zn_2GeO_4 calcined at 1323 K showed a similar absorption characteristic, but a plateau level was rather shallow. The plateau is due to the absorption by unreacted and remaining ZnO. For

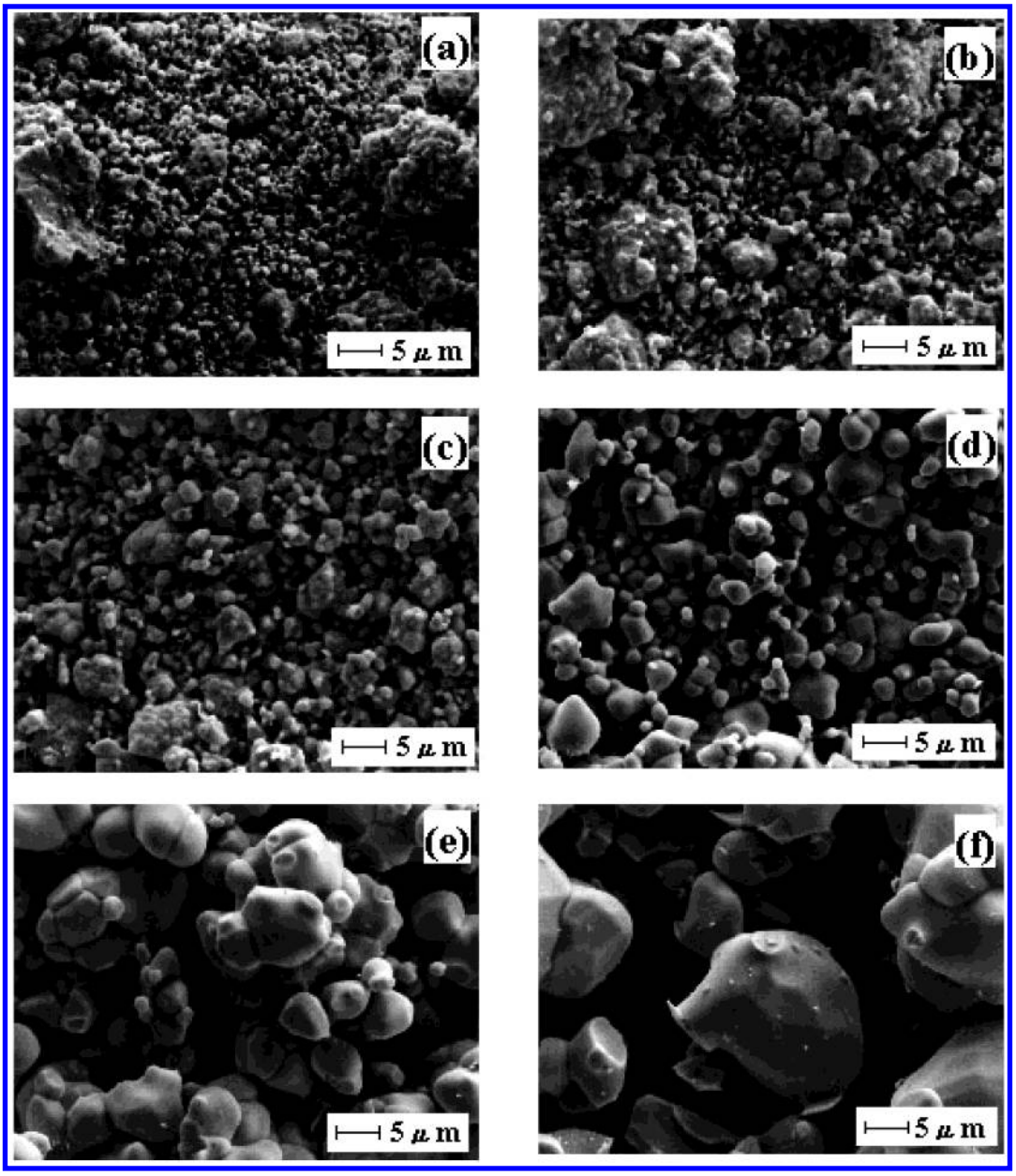

Figure 6. SEM images of Zn_2GeO_4 calcined at 1273 (a), 1323 (b), 1373 (c), 1423 (d), 1473 (e), and 1573 K (f).

Zn_2GeO_4 calcined at 1473 K, no plateau existed, and the main threshold wavelength appeared at around 310 nm. Zn_2GeO_4 calcined between 1473 and 1573 K exhibited nearly the same absorption characteristics.

Figure 6 shows scanning electron microscopic (SEM) images for Zn_2GeO_4 calcined at different temperatures. At 1323 K, round and fine particles (<1 μm) were present. With increasing calcination temperatures between 1323 and 1423 K, the particles grew significantly. Quite large growth of the particles occurred by calcination in the temperature range 1473−1573 K. The surface areas were 0.5 m^2 g^{-1} by calcination between 1273 and 1323 K and 0.4 m^2 g^{-1} between 1373 and 1473 K, and decreased to 0.2 m^2 g^{-1} above 1473 K.

Figure 7 shows the band dispersion and projected density of states (PDOS). The occupied bands are the O 2s, Ge 4s, and (Zn 3d + O 2p) bands in the increasing order of energy, and the last one is the valence band. The bottom of the conduction band is composed of the Ge 4p orbitals and small contributions of the Zn 4s4p orbitals. The band gap is estimated to be 2.0 eV.

To understand the atom-specific character in each band more clearly, PDOS is further decomposed into atomic orbital (AO) (more precisely angular momentum) contributions. Figure 8 shows AO PDOS for Zn, Ge, and O atoms. The electron density contour maps are shown in Figures 9−11 for typical bands mostly relating to photoexcitaion.

Discussion

The present study has clearly shown that RuO_2-loaded Zn_2GeO_4 makes a good photocatalyst to produce H_2 and O_2 from water with nearly the stoichiometric ratio under Hg−Xe lamp illumination. The production was reproducible in a repeated run. The photocatalytic activity was dependent on calcination temperature of Zn_2GeO_4. The dependence was similar to changes observed for the other p-block metal oxides such as MIn_2O_4 (M = Ca, Sr)[1,2,6] and $ZnGa_2O_4$.[4] The activity increased significantly between 1323 and 1473 K. In the same temperature regime, the SEM images showed that the size of Zn_2GeO_4 particles increased considerably, accompanied by narrowing of the X-ray diffraction peaks. These results dem-

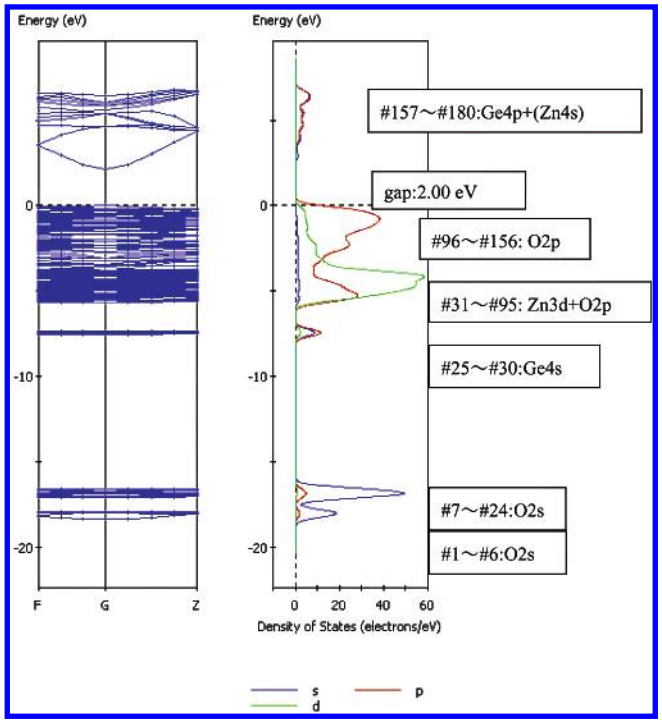

Figure 7. Band dispersion and projected density of states of Zn_2GeO_4.

onstrate that the crystallization of Zn_2GeO_4 occurs markedly over the temperature regime. This leads to the removal of impurities and structural imperfections, which is considered to be responsible for the activity enhancement. The highest activity was observed by calcination at a middle temperature of 1473 K, followed by a sharp drop of activity. In the temperature regime above 1473 K, Zn_2GeO_4 particles grew extraordinarily, as shown in the SEM images, indicative of a marked decrease in the surface area. The activity drop is evidently associated with reduction of the surface area of Zn_2GeO_4. It should be noted that the photocatalytic activity decreased at a high RuO_2 concentration, as revealed by the correlation between the amount of loaded RuO_2 and photocatalytic activity (Figure 3). This indicates that the excess amount of RuO_2 brings about agglomeration and reduces the number of photocatalytic active sites. The small surface area of Zn_2GeO_4 provides a similar situation for RuO_2 dispersion from a viewpoint of agglomeration of RuO_2 particles. The appearance of a maximum in the correlation of photocatalytic activity vs calcination temperatures of Zn_2GeO_4 indicates that the high dispersion of RuO_2 particles on well-crystallized Zn_2GeO_4 is important for better photocatalytic performance.

Metal oxide photocatalysts so far discovered for water decomposition have been composed of octahedrally coordinated d^0 transition metal ions involving Ti^{4+}, Zr^{4+}, Nb^{5+}, and Ta^{5+}. As opposed to the transition metal oxide group, our recent studies have demonstrated that RuO_2-dispersed p-block metal oxides with octahedrally coordinated d^{10} metal ions have the ability to photocatalytically decompose water to H_2 and O_2. The present findings clearly showed that Ge^{4+} metal oxides belongs to a photocatalytically active p-block metal oxide group with d^{10} configuration.

In the willemite structure of Zn_2GeO_4, the atoms are arranged in layers at six equally separated levels along the *c* axis, and each of Ge and Zn ion is in a tetrahedral environment of four oxygen atoms. One GeO_4 tetrahedron and two kinds of ZnO_4 tetrahedra are combined each other through edge oxygen. The interesting feature is that Zn_2GeO_4 consists of tetrahedrally

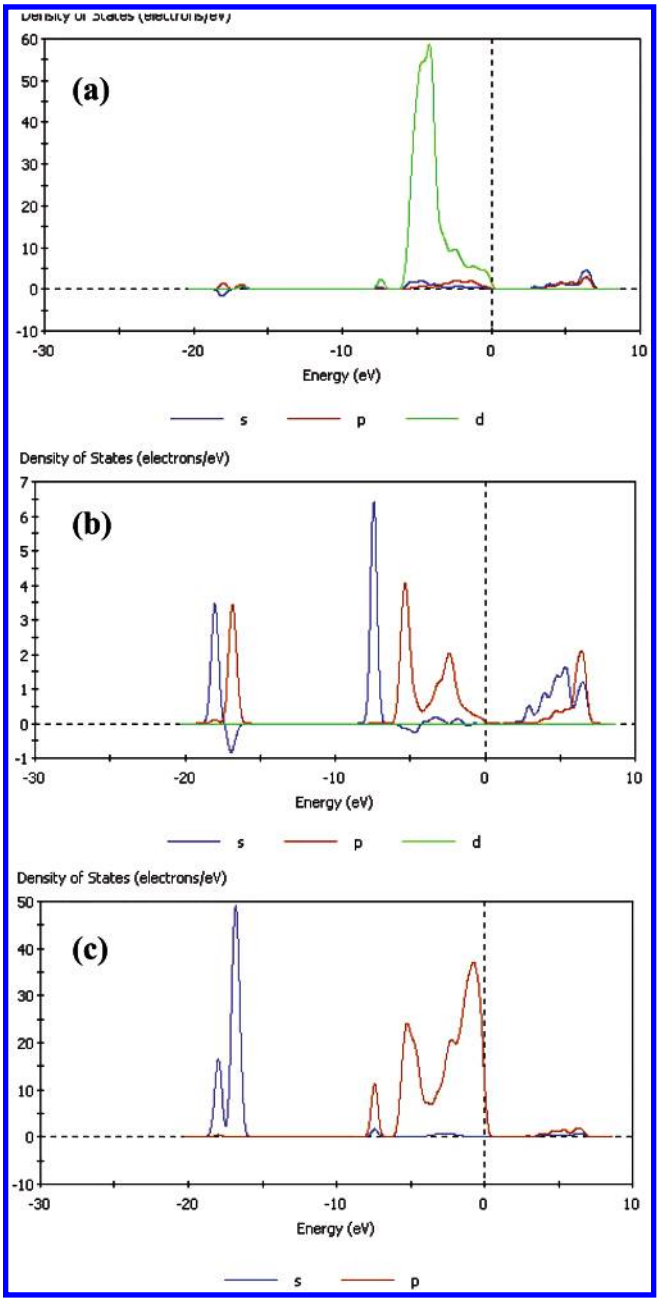

Figure 8. AO PDOS for Zn (a), Ge (b), and O (c) atom of Zn_2GeO_4.

coordinated metal ions with d^{10} configuration. To our knowledge, this is the first example of photocatalysts consisting of a tetrahedron unit that is active for water decomposition. To clarify the contributions of Ge and Zn ions to photocatalytic performance, we have investigated the photocatalytic activity of Zn_2SiO_4 with nearly the same structure of willemite. The rhombohedral cell of crystal structures is $a = 0.8626$ nm, $\alpha = 107.52°$ for Zn_2SiO_4 and $a = 0.8836$ nm and $\alpha = 107.42°$ for Zn_2GeO_4.[22] Zn_2SiO_4 has two kinds of distorted ZnO_4 tetrahedral unit, whose dipole moment is 1.1 D (D = debye) and 1.4 D. Two ZnO_4 tetrahedra in Zn_2GeO_4 are distorted and have dipole moment of 1.1 and 1.2 D. These results indicate that the two oxides have nearly the same crystal structure. As opposed to RuO_2-dispersed Zn_2GeO_4, RuO_2-loaded Zn_2SiO_4 was photocatalytically inactive. Thus, it is apparent that the tetrahedral GeO_4 is a main unit of the active sites, although the ZnO_4 unit has influences on the geometric and electronic structures of GeO_4.

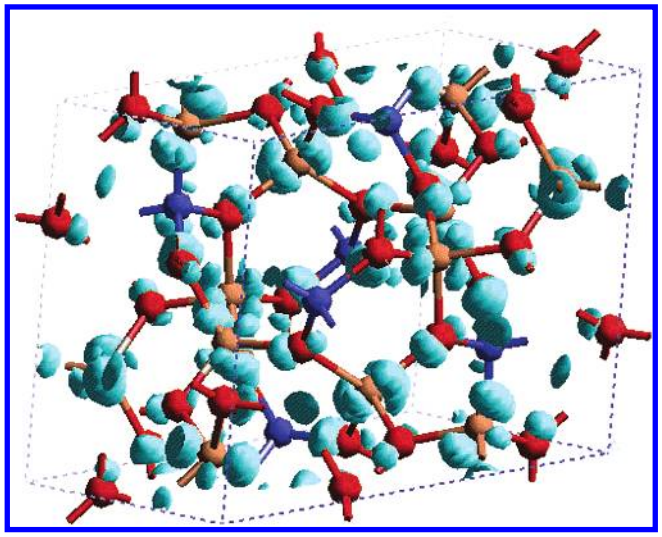

Figure 9. Electron density contour map for band #90 of valence band. Light brown, blue and red balls represent Zn, Ge, and O atom, respectively.

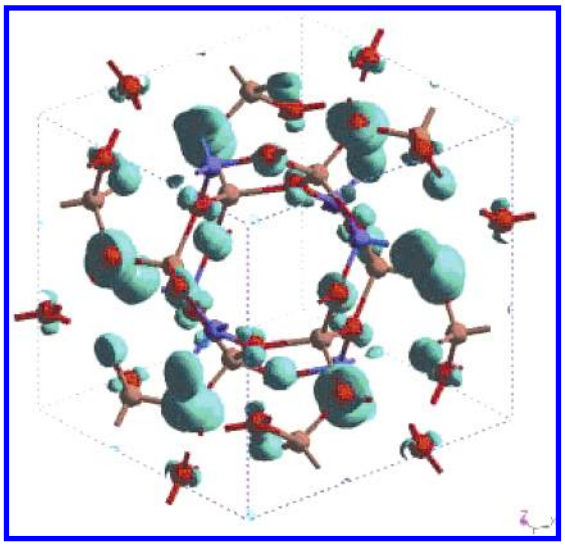

Figure 10. Electron density contour map for the top of valence band. See Figure 9 for the identification of color.

The GeO_4 tetrahedron of Zn_2GeO_4 is distorted so heavily that the center of the Ge cation deviates from the center of mass of four surrounding oxygen anions and has a dipole moment of 1.6 D inside of the tetrahedron. The correlation between the photocatalytic activity and the dipole moment has so far been demonstrated.[3,7] There are two kinds of the octahedral InO_6 in $SrIn_2O_4$: one dipole moment is 2.8 D, and the other is 1.1 D. For $Sr_{0.93}Ba_{0.07}In_2O_4$, the dipole moments are 1.70 and 2.58 D. On the other hand, $AInO_2$ (A = Li, Na) had a normal InO_6 octahedron nearly free from distortion, for which the dipole moment was zero. It has been demonstrated that $SrIn_2O_4$ and $Sr_{0.93}Ba_{0.07}In_2O_4$ consisting of distorted InO_6 octahedra with dipole moment are photocatalytically active for water decomposition when combined with RuO_2, whereas distortion-free $AInO_2$ (A = Li, Na) exhibited negligible activity.[5,6] Furthermore, $M_2Sb_2O_7$ (M = Ca, Sr), $CaSb_2O_6$, and $NaSbO_3$ with distorted SbO_6 octahedra have been shown to be photocalytically active.[3] The photocatalytic activity of RuO_2-dispersed M_2SnO_4 (M = Ca, Sr, Ba) was negligible for Ba_2SnO_4 with distortion-free SnO_6 but was markedly large for Ca_2SnO_4 and Sr_2SnO_4 consisting of distorted SnO_6. The results that the distorted tertrahedra are associated with the photocatalytic activity have been observed

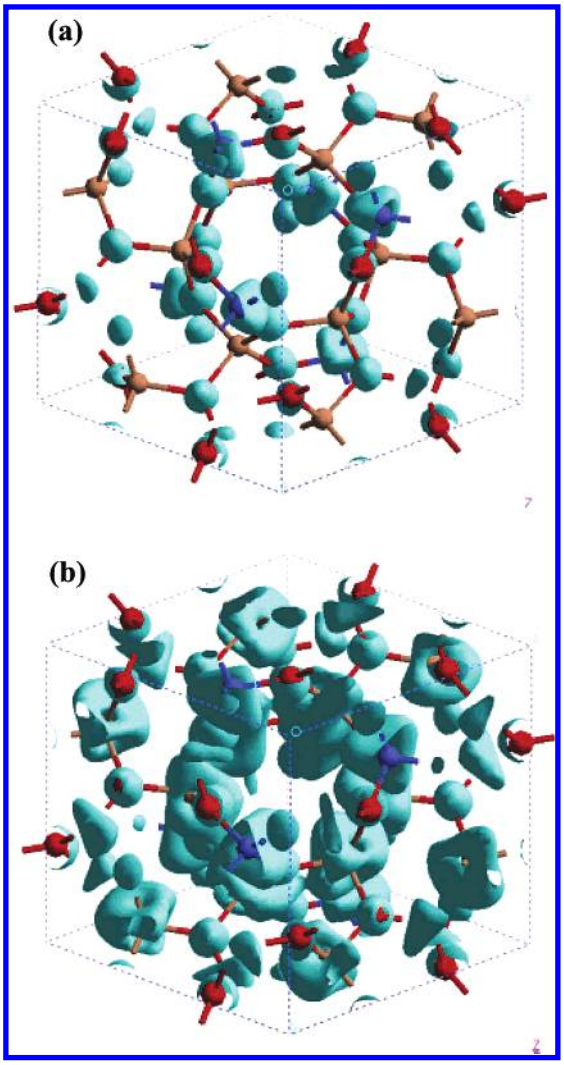

Figure 11. Electron density contour map for the bottom of conduction band at contour value of 0.1 (a) and 0.05 (b). See Figure 9 for the identification of color.

in our recent preliminary study[23] of MGa_2O_4 (M = Mg, Ca, Sr) which has demonstrated that the activity was extremely small for $MgGa_2O_4$ with normal octahedral GaO_6 but was large for $SrGa_2O_4$ and $BaGa_2O_4$ with distorted tetrahedral units.[23]

Active photocatalysts[24−26] of RuO_2-dispersed $BaTi_4O_9$ and $Na_2Ti_6O_{13}$ with d^0 configuration possess distorted TiO_6 octahedra with dipole moments of 5.7 and 4.1 D for $BaTi_4O_9$[27−29] and with dipole moments of 6.7, 5.8, and 5.3 D for $Na_2Ti_6O_{13}$.[30] Thus, it should be noted that the correlation between the photocatalytic activity and dipole moment is established for both meal oxides with d^{10} and d^0 configurations. The internal fields due to the dipole moment are considered to be useful for electron−hole separation upon photoexcitation.

As shown in Figure 7, the DFT calculation for the electronic structure of Zn_2GeO_4 demonstrates that the band dispersion is small for the occupied bands, but it is very large at the bottom of conduction band. In the core levels, the O 2s band splits into two peaks and the Ge 4s band has narrow width. The electron density contour map for the band in the middle energy range of valence band is shown in Figure 9. Both the Zn 3d and O 2p orbitals are involved. Figure 10 is the contour map for the top of valence band. The electron density is localized to the O 2p orbitals only. Thus, these results indicate that in the valence band the lower part consists of the Zn 3d and O 2p orbitals, whereas the upper part is composed of the O 2p orbitals.

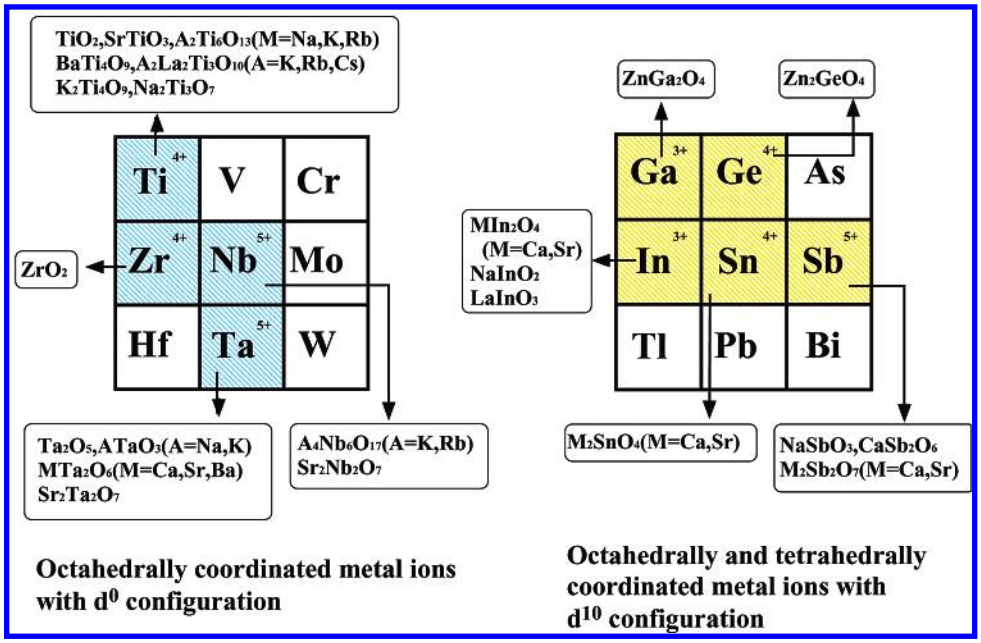

Figure 12. Conventional and new groups of photocatalysts distinguished by d^0 and d^{10} configuration.

The electron density contour map for the bottom of conduction band is shown with different contour values in Figure 11. With larger contour value (0.1), the electron density can be seen only on a Ge atom, whereas with smaller contour value (0.05), the electron density appears on both Ge and Zn atoms. The contributions of each orbital (s, p, and d orbital) of the Zn, Ge, and O atoms to the valence and conduction bands indicate that the bottom of conduction band (LUMO) is formed by the Ge 4p orbitals, and a little higher level is occupied by Ge 4s and Zn 4s4p orbitals. We can conclude that the bottom of conduction band results from the Ge 4p orbitals.

In a previous study of DFT calculation for the electronic structures of $BaTi_4O_9$ with octahedrally coordinated d^0 configuration and of $SrIn_2O_4$ with d^{10} configuration, the valence bands are similarly composed of the O 2p orbital for both the metal oxides, but the conduction band is different as shown by the Ti 3d orbital for $BaTi_4O_9$ and hybridized In 5s and 5p orbitals for $SrIn_2O_4$. The present study has shown that the conduction band is the Ge 5p orbital, and the electron transfer upon illumination occurs from the O 2p orbital to the Ge 5p orbital. Because of the large dispersion of the LUMO, the photoexcited electrons in the conduction band have large mobility, which leads to better photocatalytic performance.

In line with a model proposed previously,[7] a mechanism of photocatalysis by RuO_2-dispersed Zn_2GeO_4 can be described as follows. The internal fields due to the dipole moment of distorted GeO_4 tetrahedra promote the charge separation upon photoexcitation. The diffused Ge 5p conduction bands with large dispersion are useful for photoexcited electron transfers without recombination and permit the photoexcited electrons to move to fine RuO_2 particles dispersed on the surface as a promoter.

Figure 12 shows two groups of the photocatalysts that are active for water decomposition. One is a conventional photocatalyst consisting of transition metal oxides with d^0 configuration, and the other is a new photocatalyst group of p-block metal oxides with d^{10} configuration. In a series of our study, the concept that the p-block metal oxides having distorted octahedra and tetrahedra make good photocatalysts for water decomposition in the combination with RuO_2 has been established.

Acknowledgment. This work was supported by Solution Oriented Resarch of Science and Technology (SORST) of Japan Science and Technology(JST) Corporation and by Grant-in-Aid for Scientific Research on Priority Area (15033229) from The Ministry of Education, Science and Culture.

References and Notes

(1) Sato, J.; Saito, S.; Nishiyama, H.; Inoue, Y. *J. Phys. Chem.* **2001**, *105*, 6061.
(2) Sato, J.; Saito, S.; Nishiyama, H.; Inoue, Y.*Chem. Lett.* **2001**. 868.
(3) Sato, J.; Saito, S.; Nishiyama, H.; Inoue, Y. *J. Photochem. Photobiol. A: Chem.* **2002**, *148*, 85.
(4) Ikarashi, K.; Sato, J.; Kobayashi, H.; Saito, S.; Nishiyama, H.; Inoue, Y. *J. Phys. Chem.* **2002**, *106*, 9048.
(5) Sato, J.; Kobayashi, H.; Saito, S.; Nishiyama, H.; Inoue, Y. *J. Photochem. Photobio A: Chem.* **2002**, *148*, 85.
(6) Sato, J.; Saito, S.; Nishiyama, H.; Inoue, Y. *J. Phys. Chem. B* **2003**, *107*, 7965.
(7) Sato. J.; Kobayashi, H.; Inoue, Y. *J. Phys. Chem. B* **2003**, *107*, 7970.
(8) Domen, K.; Kudo, A.; Onishi, T. *J. Catal*. **1986**, *102*, 92.
(9) Inoue, Y.; Kubokawa, T.; Sato, K. *J. Phys. Chem*. **1991**, *95*, 4059.
(10) Ogura, S.; Kohno, M.; Sato, K.; Inoue, Y. *Appl. Surf. Sci*. **1997**, *121/123*, 521.
(11) Inoue, Y.; Asai, Y.; Sato, K. *J. Chem. Soc., Faraday Trans.* **1994**, *90*, 797.
(12) Kohno, M.; Kaneko, T.; Ogura, S.; Sato, K.; Inoue, Y. *J. Chem. Soc., Faraday Trans.* **1998**, *94*, 89.
(13) Takata, T.; Furumi, Y.; Shinohara, K.; Tanaka, A.; Hara, M.; Kondo, J. N.; Domen, K. *Chem. Mater*. **1997**, *9*, 1063.
(14) Takata, T.; Shinohara, K.; Tanaka, A.; Hara, M.; Kondo, J. N.; Domen, K. *J. Photochem. Photobiol. A: Chem*. **1997**, *106*, 45.
(15) Sayama, K.; Arakawa, H. *J. Phys. Chem*. **1993**, *97*, 531.
(16) Kudo, A.; Tanaka. A.; Domen, K.; Maruya, K.; Aika, K.; Onishi, T. *J. Catal.* **1998**, *111*, 67.
(17) Kudo, A.; Kato, H.; NakaGawa, S. *J. Phys. Chem. B* **2000**, *104*, 571.
(18) Kato, H.; Kudo, A. *Catal. Lett*. **1999**, *58*, 153.
(19) Ishihara, T.; Nishiguchi, H.; Fukamachi, K.; Takita, Y. *J. Phys. Chem. B* **1999**, *103*, 1.
(20) Kato, H.; Kudo, A. *Chem. Phys. Lett*. **1998**, *295*, 487.
(21) Kato, H.; Kudo, A. *Chem. Lett*. **1999**, 1027.
(22) Hang, C.; Simonov, M. A.; Belov, N. V. *Soviet Phys. Crystallogr*. **1970**, *15*, 387.
(23) Unpublished data.
(24) Inoue, Y.; Asai, Y.; Sato, K. *J. Chem. Soc., Faraday Trans*. **1994**, *90*, 797. Kohno, M.; Ogura, S.; Sato, K.; Inoue, Y. *Chem. Phys. Lett*. **1997**, *267*, 72.

(25) Inoue, Y.; Kubokawa, T.; Sato, K. *J. Phys. Chem*. **1991**, *95*, 4059.
(26) Ogura, S.; Kohno, M.; Sato, K., Inoue, Y. *Phys. Chem. Chem. Phys*. **1999**, *1*, 179.
(27) Lukaszewicz, K. *Roez. Chem*. **1957**, *31*, 1111.
(28) Templeton, D. H.; Dauben, C. H. *J. Chem. Phys*. **1960**, *32*, 1515.
(29) Hofmeister, W.; Tillmanns, E.; Baur W. H. *Acta Crystallogr*. **1984**, *C 40*, 1510.
(30) Andersson, S.; Wadsley, A. D. *Acta Crystallogr*. **1962**, *15*, 194.